



## Experimental observation of front propagation in a negatively diffractive inhomogeneous Kerr cavity

V. Odent,<sup>1,2,\*</sup> M. Tlidi,<sup>3</sup> M. G. Clerc,<sup>2</sup> P. Glorieux,<sup>1,†</sup> and E. Louvergneaux<sup>1</sup>

<sup>1</sup>Laboratoire de Physique des Lasers, Atomes et Molécules, CNRS UMR8523, Université Lille1, 59655 Villeneuve d'Ascq Cedex, France

<sup>2</sup>Departamento de Física, FCFM, Universidad de Chile, Blanco Encalada 2008, Santiago, Chile

<sup>3</sup>Faculté des Sciences, Université Libre de Bruxelles, CP 231, Campus Plaine, B-1050 Bruxelles, Belgium

(Received 11 February 2014; published 22 July 2014)

A focusing Kerr Fabry-Pérot cavity operating in a negative diffraction regime exhibits transverse propagating fronts connecting two different nematic liquid crystal molecule average orientations. Under an inhomogeneous spatial pumping beam, these fronts stop to propagate and lead to the formation of a stable localized structure. The trajectory of the front position is derived from the mean-field model. Its hyperbolic tangent analytical expression perfectly fits the experimental data.

DOI: [10.1103/PhysRevA.90.011806](https://doi.org/10.1103/PhysRevA.90.011806)

PACS number(s): 42.65.Hw, 42.25.Fx, 45.70.Qj

**Introduction.** The formation of dissipative structures far from equilibrium has motivated many studies since the pioneering work of Turing [1] and Prigogine and Lefever [2]. It concerns almost all fields in natural science such as biology, chemistry, ecology, physics, fluid mechanics, and optics. In particular, the formation of localized structures (LSs) and localized patterns that belong to this class of structures has been a subject of intense research (see reviews on this issue [3,4] and references therein). They consist of localized peaks in one or more spatial dimensions. When they are sufficiently separated from each other, localized peaks are independent and randomly distributed in space. The prerequisite condition for spatial confinement leading to the formation of LSs is the occurrence of subcritical modulational or Turing instability where a coexistence between a homogeneous background and a self-organized periodic structure occurs [5–9]. Several experiments have been realized with the aim of a future application as pixel bits in optical memories [10–16]. This issue has been widely discussed and is by now fairly well understood.

In another line of research it is known that many systems could operate in the negative (or anomalous [17]) diffraction regime. The periodic modulation of the refraction index allows one to invert the sign of the diffraction coefficient [18] in atomic Bose-Einstein condensates [19] and in dissipative nonlinear photonic crystal resonators [20–25]. Another example of negative diffraction systems is the near self-imaging resonators [26] and more recently left-handed materials [27–32]. The case of zero diffraction has also been investigated [33].

In this Rapid Communication we consider a focusing driven Kerr Fabry-Pérot cavity. We show experimentally the occurrence of stable localized structures in a modulationally stable regime, i.e., in a regime far from any modulational or Turing instability [1,2]. We attribute the stabilization of these solutions to the combined action of negative diffraction and an inhomogeneous pumping laser beam. It has been shown that the laser cavity can also be considered as an inhomogeneous cavity [34,35]. In the short time evolution, fronts connecting two different nematic liquid crystal molecule average orientations counterpropagate. The final optical permanent state is composed of two bounded fronts forming a stable LS. The hyperbolic tangent trajectory of the front core under Gaussian forcing is predicted from a Lugiato-Lefever (LL) model [36] that perfectly fits the experimental data. Since optical cavities are a basic configuration in nonlinear systems and since localized structure formation [3,4] and front propagation [5,37] are ubiquitous phenomena in nonlinear science, our observations are liable to be relevant to other fields of research such as photonics crystals or left-handed materials.

**Experimental setup.** The experiments have been carried out using a nonlinear Kerr slice medium inserted in an optical Fabry-Pérot resonator. The Kerr focusing medium is a 50- $\mu\text{m}$ -thick layer of E7 nematic liquid crystal homeotropically anchored. Two plane mirrors  $M_1$  and  $M_2$  define the physical cavity. An intracavity  $4f$  lens arrangement ( $L_1$  and  $L_2$  in Fig. 1) images in  $M'_2$  the real mirror  $M_2$ . Consequently, the equivalent optical cavity is delimited by  $M_1$  and  $M'_2$  (see Fig. 1). Its optical length  $d$  may be tuned from positive to negative values (positive in Fig. 1). Thus, for negative optical cavity path ( $d < 0$ ), a beam propagating along this path experiences negative diffraction. Together with the positive Kerr index, the experimental setup is then equivalent to a Kerr cavity that would have a positive optical distance but negative Kerr index (the  $\eta a$  product sign in Ref. [36] that defines the type of transverse instabilities remains the same). However, the physical mechanisms of negative refraction and negative diffraction are different. Thus, this intracavity geometrical lens arrangement allows for achieving an equivalent left-handed Kerr material in the visible range. It also allows one to continuously tune the diffraction from positive to negative.

The experimental cavity finesse is 11.6 [15]. The cavity is pumped with a beam delivered by a single-mode frequency-doubled  $\text{Nd}^{3+}:\text{YVO}_4$  laser ( $\lambda_0 = 532 \text{ nm}$ ) that is shaped by means of two cylindrical telescopes. The resulting beam size ( $\sim 200 \times 2800 \mu\text{m}^2$ ) gives a cylindrical transverse shape such that only one spot can develop in one of the two directions. The system may then be considered as one dimensional. The beam propagating in the forward direction is monitored at the output of  $M_2$  mirror. In addition to  $d$ , two control parameters are easily accessible in the experiments, namely, the maximum input intensity  $I_0$  of the incident laser beam and the cavity detuning via the linear phase shift  $\varphi$  of one cavity round-trip. As the

As the

\*vodent@ing.uchile.cl

†Deceased.

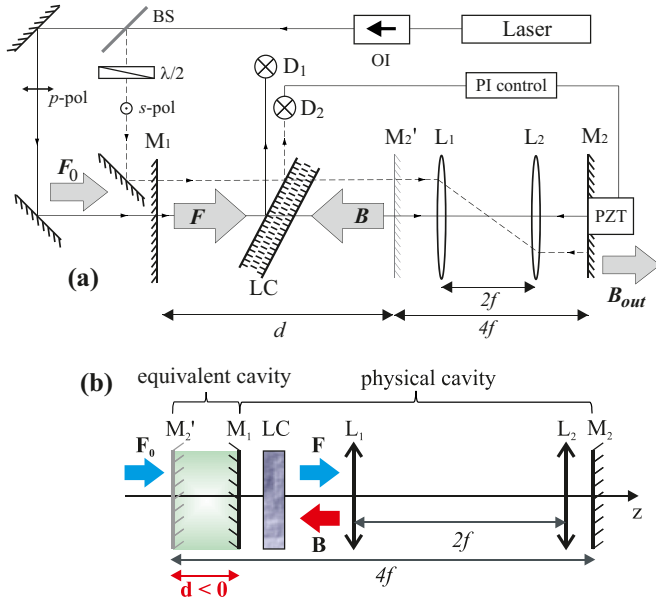


FIG. 1. (Color online) Inhomogeneous Kerr cavity with negative diffraction. (a) Experimental setup. (b) Schematic representation of the physical cavity and the equivalent cavity: OI is the optical isolator; BS is the beam splitter; LC is the liquid crystal slice;  $D_1$  and  $D_2$  are photodetectors;  $L_1$  and  $L_2$  are lenses of focal length  $f$ ;  $p$  and  $s$  are the polarized components of the pump (solid line) and probe (dashed line) beams, respectively; and  $M_1$  and  $M_2$  are the real cavity mirrors but the optical Fabry-Pérot cavity is delimited by  $M_1$  and  $M_2'$  mirrors and its length is  $d$ .

dynamical regimes are highly dependent on the value of  $\varphi$ , the optical cavity length is actively stabilized using a very weak probe beam orthogonally polarized to the main beam [15].

Our cavity inserting a Kerr focusing nonlinearity is tuned such that (i) it operates in the bistable regime ( $\varphi < 0$ ), where the states correspond to different nematic liquid crystal molecule average orientations, and (ii) it experiences negative diffraction ( $d < 0$ ). The remaining control parameter here is the injected optical power. For low power [ $t < 0$  in Fig. 2(c)] (corresponding to the lower branch of the cavity transfer function bistability cycle), the transmitted intensity profile mimics the input Gaussian transverse beam shape. As the input power is suddenly increased to the upper bistability response branch ( $t = 0$  s), the central part of the transmitted intensity profile suddenly jumps after some latency time [ $t \approx 37$  s in Fig. 2(c)] to a higher value and invades the surroundings towards the external regions where the field is less intense before stopping its propagation. Finally, the fronts lock to give a localized light state [Fig. 2(e)]. Changing the waist  $w$  of the Gaussian forcing or its intensity within the bistability region allows one to tune the distance between the bounded fronts and thus the localized state extension.

A transverse cut of the transmitted intensity profile is depicted in Fig. 2(a), obtained in the initial and the final observation period. This figure emphasizes the coexistence of different states in the same region of parameters. In addition, one state emerges from the other because of the inherent fluctuations of the system. Figure 2(c) shows this phenomenon starting at  $t \approx 37$  s. From this instant, the system exhibits two counterpropagating fronts, which will become asymptotically

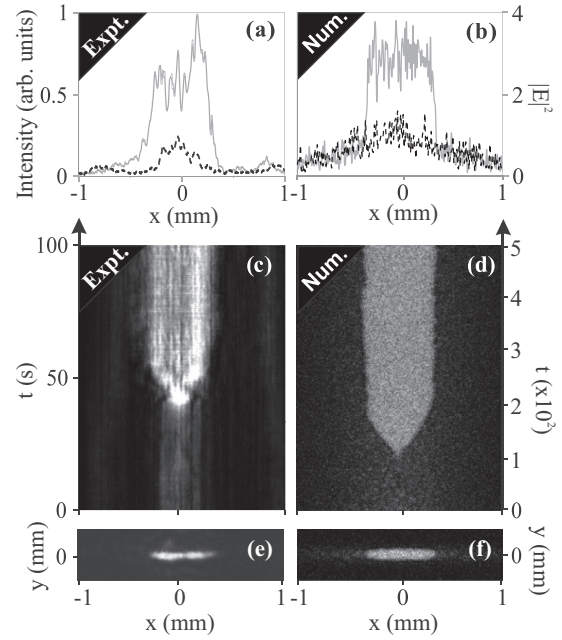


FIG. 2. Front propagation in the negative diffractive inhomogeneous Kerr cavity. (a) and (b) Transverse cross section of the initial (final) average localized structure shown by the dashed black (solid gray) line. (c) and (d) Spatiotemporal response to a step function of the input intensity from the lower to the upper branch of the bistable cycle. (e) and (f) Experimental and numerical cross section of the localized state. Light region account for high intensity of the light. (a), (c), and (e) Experiments with  $I_0 = 433 \text{ W cm}^{-2}$ ,  $d = -5 \text{ mm}$ ,  $\varphi = -0.6$  rad,  $w_x = 1400 \mu\text{m}$ ,  $w_y = 100 \mu\text{m}$ ,  $R_1 = 81.8\%$ , and  $R_2 = 81.4\%$ . (b) and (d) Numerical simulation of the LL model with  $E_0 = 1.9$ ,  $\Delta = 3.0$ ,  $\alpha = 0.001$ ,  $w_x = 1400 \mu\text{m}$ ,  $w_y = 100 \mu\text{m}$ , and  $\varepsilon = 0.4$ .

motionless [see Fig. 2(c)]. The motionless front is observed at the location  $x_0(\text{expt}) \cong \pm 0.17w$ . At this location, the input intensity is only 3% lower than at the center of the input beam. Thus, we observe experimentally the coexistence between two inhomogeneous states; the noise induces a pair of fronts between these states, which initially counterpropagate until asymptotically they stop.

*Theoretical description.* In the mean-field limit, the dynamics of the single longitudinal mode of the bistable system that consists of a Fabry-Pérot cavity filled with a liquid crystal Kerr-like medium and driven by a coherent plane-wave steady state can be described by the simple partial differential equation (the LL model [36])

$$\frac{\partial E}{\partial t} = E_{\text{in}}(x) - (1 + i\Delta)E + i|E|^2E - i|\alpha| \frac{\partial^2 E}{\partial x^2}, \quad (1)$$

which includes the effect of diffraction, which is proportional to  $\alpha$ . Here  $E$  is the normalized slowly varying envelope of the electric field,  $\Delta$  is the detuning parameter, and  $E_{\text{in}}$  is the input field assumed to be real, positive, and spatially inhomogeneous. The negative diffraction coefficient is  $|\alpha|$ . Note that the above model has been derived for a cavity filled with left-handed material operating in the negative diffraction regime [29].

At the onset of optical bistability, there is a second-order critical point where the output versus input characteristics has

an infinite slope. The critical detuning at the onset of optical bistability is  $\Delta = \Delta_c \equiv \sqrt{3}$ . In order to study the dynamics of the front connecting the two homogeneous steady states, we explore the vicinity of the critical point associated with bistability. For this purpose, we introduce a small parameter that measures the distance from the critical point  $\zeta \ll 1$  and we express the cavity detuning in the form  $\Delta = \Delta_c(1 + \zeta^2\sigma)$ , where  $\sigma$  is a quantity of order one. Then we decompose the envelope of the electric field into its real and imaginary parts  $E = x_1 + ix_2$  and we introduce new space and time scales as  $(x, t) \rightsquigarrow [\zeta^2 t / \sigma, 3^{1/4} \zeta x / (|\alpha| \sqrt{\sigma})]$ . Let  $(X_1, X_2, Y_{\text{in}}) = (x_1, x_2, E_{\text{in}}) - (3/4, \sqrt{3}/4, 1)E_{\text{in}}^c$ , with  $E_{\text{in}}^c = 2\sqrt{2}/3^{3/4}$ , be the deviations of the real and imaginary cavity fields and of the injected field with respect to the values of these quantities at the critical point. Our aim is to seek solutions of Eq. (1) in the neighborhood of the critical point associated with the optical bistability. To this end, we expand the cavity field and the injected field as  $(X_1, X_2, Y_{\text{in}}) = \zeta[(u_0, v_0, y_0) + \zeta(u_1, v_1, y_1) + \zeta^2(u_2, v_2, y_2) + \dots]$ . Inserting this expansion into the LL model and using the above scalings, we then obtain a hierarchy of linear problems for the unknown functions. At the first order in  $\zeta$ , we find  $Y_0 = 0$  and  $u_0 = -w_0$ . At the second we have  $Y_1 = 3\sigma/4$ . Finally, at the third order, the solvability condition yields

$$\frac{\partial u}{\partial t} = \eta + u - u^3 + \frac{\partial^2 u}{\partial x^2}, \quad (2)$$

where  $u(x, t) = \sqrt{3/2\sigma}u_0$  is a scalar field that accounts for the real part of the envelope  $E$  and  $\eta = 4y_2\sigma/3$  controls the relative stability between the equilibria. Note that  $y_2$  is proportional to the pumping  $E_{\text{in}}$ . Hence, if the pumping is inhomogeneous then the parameter  $\eta$  is also inhomogeneous. For a Gaussian pumping, we consider

$$\eta(x) \equiv \tilde{\eta} + \eta_0 e^{-(x/w)^2}, \quad (3)$$

where  $\eta_0$  accounts for the strength of the spatial pumping beam and  $w$  is the width of the Gaussian. For  $\eta(x) = 0$  both states are symmetric corresponding to the Maxwell point, where a front between these states is motionless.

The above model (2) describes the appearance of bistability in an inhomogeneous medium [6]. From the bifurcation point of view, this equation accounts for an extended inhomogeneous imperfect pitchfork bifurcation [38]. To perform analytical developments, we first approximate the Gaussian forcing by a parabola (first-order development close to the center of the optical pumping where the stress is maximum), that is,  $\eta(x) \approx -\tilde{\eta} + \eta_0[1 - (x/w)^2]$ . Close to the Maxwell point, one can consider the following ansatz for the front solution:  $u(x, t) = \tanh\{[x - x_0(t)]/\sqrt{2}\} + W$ , where  $x_0$  stands for the front position. This position is promoted to a function of time to account for the effects of inhomogeneity and asymmetry among states. In addition,  $W$  accounts for small corrections. To get the front dynamic, we introduce the above ansatz for  $u$  in Eq. (2), linearizing in  $W$  and imposing the solvability condition, to obtain

$$\dot{x}_0 = \frac{-3\sqrt{2}}{2} \left\{ -\tilde{\eta} + \eta_0 \left[ 1 - \left( \frac{x_0}{w} \right)^2 - \left( \frac{\pi}{\sqrt{6}w} \right)^2 \right] \right\}, \quad (4)$$

which leads to the trajectory of the front

$$x_0(t) = \pm a \tanh[b(t - t_0)], \quad (5)$$

where  $a$ ,  $b$ , and  $t_0$  are coefficients depending on  $\eta_0$ ,  $\tilde{\eta}$ , and  $w$ . The equilibrium position of the front  $x_{0\infty}$  can be inferred from the expression (5) for  $t \rightarrow \infty$  as  $x_{0\infty} = \pm w \sqrt{1 - \tilde{\eta}/\eta_0}$ . This equilibrium position could be obtained directly from Eq. (2), assuming  $\eta(x_{0\infty}) = 0$ , which is the condition for the motionless front (Maxwell point). Extending this last property to the initial Gaussian forcing, we get

$$x_{0\infty} = \pm w \sqrt{\ln \left( \frac{\eta_0}{\tilde{\eta}} \right)}. \quad (6)$$

At the leading order, Eq. (6) recovers again the previous expression of  $x_{0\infty}$  for the parabolic approximation of the Gaussian profile.

Numerical simulations of the LL model (1) under parabolic as well as Gaussian spatial forcing show perfect agreement with the front position dynamics (5). In order to perform more realistic numerical simulations, we have conducted simulations in two dimensions with a asymmetric Gaussian forcing with a cylindrical shape ( $w_x \gg w_y$ ). That is, we consider

$$E_{\text{in}}(x, y) = E_0 \exp \left\{ - \left[ \left( \frac{x}{w_x} \right)^2 + \left( \frac{y}{w_y} \right)^2 \right] \right\}. \quad (7)$$

Furthermore, we have included the inherent fluctuations of the system by adding a stochastic term (white noise) with noise intensity  $\epsilon$ . Numerical simulations with these ingredients show

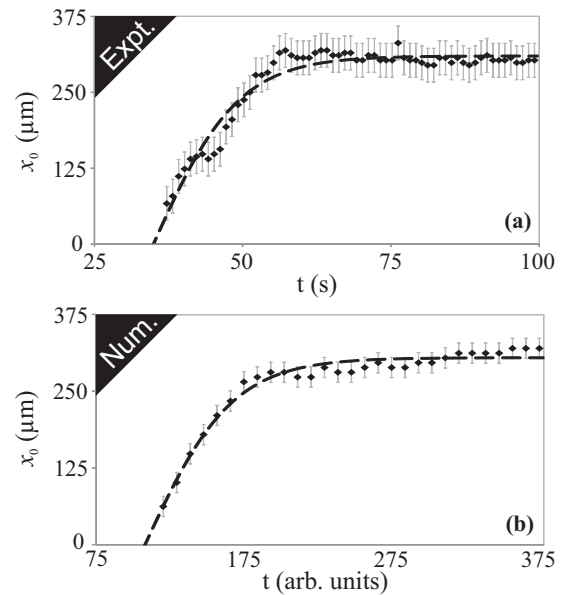


FIG. 3. Temporal evolution of the front position  $x_0(t)$  corresponding to the spatiotemporal diagrams of Fig. 2. (a) Experiment and (b) numerical simulations of the LL model (1) using the same parameters considered in Fig. 2. Diamonds represent the location values extracted from the smoothed spatiotemporal diagrams. Dashed curves are the best fit using expression (5). The experimental fit parameters are  $a = 308 \mu\text{m}$ ,  $b = 0.069$ , and  $t_0 = 35.2 \text{ s}$ ; the numerical fit parameters are  $a = 306 \mu\text{m}$ ,  $b = 0.017$ , and  $t_0 = 107.7$ .

quite good agreement, in terms of the structure profile, front dynamics, and two-dimensional shape [see Figs. 2(b), 2(d), and 2(f)], with the experimental observations [see Figs. 2(a), 2(c), and 2(e)]. Hence, the analytical expression (5) can be used to figure out and to characterize the experimental front dynamics. Figure 3 depicts the experimental and numerical temporal evolutions of the position of the front. It clearly evidences that the expression of Eq. (5) reproduces the dynamics of the front. Therefore, the effect of a spatial forcing on front propagation is to induce the front moves and stops on an asymptotic position, satisfying a hyperbolic tangent trajectory.

**Conclusion.** Using a geometrical arrangement, we show how to generate an equivalent left-handed Kerr material in the visible range. Experimentally, we show that the nonlinear dynamical states appearing in a focusing Kerr Fabry-Pérot cavity submitted to negative optical feedback are propagating fronts in an inhomogeneous medium. Theoretically, the system is modeled, in the mean-field limit, by a single longitudinal mode that describes an oscillatory forcing inhomogeneous nonlinear diffracted medium, the LL model. From this model we have derived a simple bistable model with inhomogeneous

parameters. The inhomogeneous spatial forcing coming from the optical Gaussian pumping generates, experimentally and theoretically, the front moves and stops on an asymptotic position. The experimental trajectory of the front position under that forcing follows a hyperbolic tangent law that fully agrees with the prediction from a generic bistable imperfect pitchfork bifurcation model. As a consequence of the Gaussian forcing, the system exhibits a localized state as equilibrium. This state is composed of two opposite fronts.

**Acknowledgments.** The authors thank S. Coulibaly and M. Taki for stimulating discussions. The authors acknowledge financial support from the ANR International program, Project No. ANR-2010-INTB-402-02 (ANRCONICYT39), COLORS. M.G.C. thanks FONDECYT for financial support through Project No. 1120320. This research was also supported in part by the Centre National de la Recherche Scientifique, the Fonds Européen de Développement Economique de Régions, and the Interuniversity Attraction 463 Poles program of the Belgian Science Policy Office, under 464 Grant No. IAP P7-35 Photonics@be.

- 
- [1] A. Turing, *Philos. Trans. R. Soc. London* **237**, 37 (1952).  
 [2] I. Prigogine and R. Lefever, *J. Chem. Phys.* **48**, 1695 (1968).  
 [3] D. Mihalache *et al.*, *Prog. Opt.* **27**, 229 (1989); N. N. Rosanov, *Spatial Hysteresis and Optical Patterns* (Springer, Berlin, 2002); L. A. Lugiato, *IEEE J. Quantum Electron.* **39**, 193 (2003); J. D. Murray, *Mathematical Biology*, 3rd ed. (Springer, Berlin, 2003); Y. S. Kivshar and G. P. Agrawal, *Optical Solitons: From Fiber to Photonic Crystals* (Academic, New York, 2003); K. Staliūnas and V. J. Sánchez-Morcillo, *Transverse Patterns in Nonlinear Optical Resonators*, Springer Tracts in Modern Physics Vol. 183 (Springer, Berlin, 2003); P. Mandel and M. Tlidi, *J. Opt. B* **6**, R60 (2004); A. Malomed *et al.*, *ibid.* **7**, R53 (2005); A. S. Mikhailov and K. Showalter, *Phys. Rep.* **425**, 79 (2006).  
 [4] G. Purwins *et al.*, *Adv. Phys.* **59**, 485 (2010); O. Descalzi, M. Clerc, S. Residori, and G. Assanto, *Localized States in Physics: Solitons and Patterns* (Springer, New York, 2011); M. Peckus, R. Rogalskis, V. Sirutkaitis, and K. Staliūnas, *Lith. J. Phys.* **53**, 25 (2013).  
 [5] Y. Pomeau, *Physica D* **23**, 3 (1986).  
 [6] M. Tlidi, P. Mandel, and R. Lefever, *Phys. Rev. Lett.* **73**, 640 (1994); A. J. Scroggie, W. J. Firth, G. S. McDonald, M. Tlidi, R. Lefever, and L. A. Lugiato, *Chaos Solitons Fractals* **4**, 1323 (1994).  
 [7] M. Brambilla, L. A. Lugiato, and M. Stefani, *Europhys. Lett.* **34**, 109 (1996).  
 [8] P. Couillet, *Int. J. Bifurcat. Chaos* **12**, 2445 (2002).  
 [9] M. G. Clerc and C. Falcon, *Physica A* **356**, 48 (2005).  
 [10] V. B. Taranenko, K. Staliūnas, and C. O. Weiss, *Phys. Rev. Lett.* **81**, 2236 (1998).  
 [11] V. B. Taranenko, I. Ganne, R. Kuszelewicz, and C. O. Weiss, *Appl. Phys. B* **72**, 377 (2001).  
 [12] S. Barland *et al.*, *Nature (London)* **419**, 699 (2002).  
 [13] F. Haudin, R. G. Elias, R. G. Rojas, U. Bortolozzo, M. G. Clerc, and S. Residori, *Phys. Rev. Lett.* **103**, 128003 (2009).  
 [14] M. G. Clerc, F. Haudin, S. Residori, U. Bortolozzo, and R. G. Rojas, *Eur. Phys. J. D* **59**, 43 (2010).  
 [15] V. Odent, M. Taki, and E. Louvergneaux, *New J. Phys.* **13**, 113026 (2011).  
 [16] E. Averlant, M. Tlidi, H. Thienpont, T. Ackemann, and K. Panajotov, *Opt. Express* **22**, 762 (2014).  
 [17] We refer here to the term anomalous in reference to “anomalous dispersion” in temporal dynamics; see, e.g., G. P. Agrawal, *Nonlinear Fiber Optics*, 3rd ed. (Academic, New York, 2001).  
 [18] D. N. Cristodoulides and R. I. Joseph, *Opt. Lett.* **13**, 794 (1988); A. Aceves *et al.*, *Phys. Rev. E* **53**, 1172 (1996); F. Lederer *et al.*, *Discrete Solitons* (Springer, New York, 2001).  
 [19] Y. S. Kivshar *et al.*, *Phys. Lett. A* **278**, 225 (2001); B. Eiermann *et al.*, *Phys. Rev. Lett.* **91**, 060402 (2003).  
 [20] M. Notomi, *Phys. Rev. B* **62**, 10696 (2000).  
 [21] K. Staliūnas, *Phys. Rev. Lett.* **91**, 053901 (2003).  
 [22] D. N. Neshev *et al.*, *Phys. Rev. Lett.* **92**, 123903 (2004).  
 [23] C. Conti and S. Trillo, *Phys. Rev. Lett.* **92**, 120404 (2004).  
 [24] K. Staliūnas and R. Herrero, *Phys. Rev. E* **73**, 016601 (2006).  
 [25] D. Gomila and G.-L. Oppo, *Phys. Rev. A* **76**, 043823 (2007).  
 [26] J. A. Arnaud, *Appl. Opt.* **8**, 189 (1969).  
 [27] G. D’Aguanno, N. Mattiucci, M. Scalora, and M. J. Bloemer, *Phys. Rev. Lett.* **93**, 213902 (2004).  
 [28] P. Kockaert, P. Tassin, G. Van der Sande, I. Veretennicoff, and M. Tlidi, *Phys. Rev. A* **74**, 033822 (2006).  
 [29] P. Tassin, G. V. der Sande, N. Veretenov, P. Kockaert, I. Veretennico, and M. Tlidi, *Opt. Express* **14**, 9338 (2006).  
 [30] P. Tassin, L. Gelens, J. Danckaert, I. Veretennicoff, G. Van der Sande, P. Kockaert, and M. Tlidi, *Chaos* **17**, 037116 (2007).  
 [31] A. Boardman, M. Brongersma, M. Stockman, and M. Wegener, *J. Opt. Soc. Am. B* **26**, PM1 (2009).  
 [32] M. Tlidi, P. Kockaert, and L. Gelens, *Phys. Rev. A* **84**, 013807 (2011).

- [33] S. Residori, A. Petrossian, T. Nagaya, C. S. Riera, and M. G. Clerc, *Physica D* **199**, 149 (2004).
- [34] H. Zhang, D. Y. Tang, L. M. Zhao, and X. Wu, *Phys. Rev. B* **80**, 052302 (2009).
- [35] H. Zhang, D. Y. Tang, L. Zhao, and X. Wu, *Opt. Express* **19**, 3525 (2011).
- [36] L. A. Lugiato and R. Lefever, *Phys. Rev. Lett.* **58**, 2209 (1987).
- [37] L. M. Pismen, *Patterns and Interfaces in Dissipative Dynamics* (Springer, Berlin, 2006).
- [38] S. Strogatz, *Nonlinear Dynamics and Chaos: With Applications to Physics, Biology, Chemistry and Engineering* (Addison-Wesley, Reading, MA, 1994).